

# **Stochastic Pharmacokinetic-Pharmacodynamic Modeling for Assessing the Systemic Health Risk of Perfluorooctanoate (PFOA)**

## **– Supplementary Information –**

**Matteo Convertino<sup>1,2,3,4</sup>, Timothy R. Church<sup>4,5</sup>, Geary W. Olsen<sup>6</sup>, Yang Liu<sup>1</sup>, Eddie Doyle<sup>7</sup>, Clifford R. Elcombe<sup>7,10</sup>, Anna L. Barnett<sup>7</sup>, Leslie M. Samuel<sup>8</sup>, Iain R. MacPherson<sup>9</sup>, Thomas R. J. Evans<sup>9</sup>**

<sup>1</sup> School of Public Health, Division of Environmental Health Sciences & Public Health Informatics Program, HumNat Lab, University of Minnesota, Minneapolis, MN, USA

<sup>2</sup> Institute on the Environment, University of Minnesota, St. Paul, MN, USA

<sup>3</sup> Institute for Engineering in Medicine, University of Minnesota, Minneapolis, MN, USA

<sup>4</sup> School of Public Health, Division of Environmental Health Sciences, University of Minnesota, Minneapolis, MN, USA

<sup>5</sup> Masonic Cancer Center, University of Minnesota, Minneapolis, MN, USA

<sup>6</sup> Medical Department, 3M Company, St. Paul, MN, USA

<sup>7</sup> CXR Biosciences, Dundee, United Kingdom

<sup>8</sup> Aberdeen Royal Infirmary, Aberdeen, United Kingdom

<sup>9</sup> Institute of Cancer Sciences, CR-UK Beatson Institute, University of Glasgow, Glasgow, United Kingdom

<sup>10</sup> Deceased

Keywords: PFOA, PKPD modeling, biomarkers, networks, cholesterol, fT4, Phase 1

Corresponding authors: [matteo@ist.hokudai.ac.jp](mailto:matteo@ist.hokudai.ac.jp), [trc@umn.edu](mailto:trc@umn.edu)

## **Analytical Measurement of PFOA**

For the 49 subjects and their collective weekly samples, plasma (40 µL) was pipetted into a 2.2 mL polypropylene tube, diluted with 1.56 mL methanol and vortex mixed. The mixed sample was then centrifuged at approximately 13,000 g for 10 minutes. An 80 µL aliquot of the supernatant was then transferred to a 500 µL Eppendorf tube, internal standard solution added (20 µL; 13C-ammonium perfluorooctanoate, 500 ng/mL in methanol) and vortex mixed. The sample extract (100 µL) was then transferred to 96 well plate and 10 µL injected into the LC/MS/MS.

Chromatographic separation was carried out using a Waters Alliance HT2795 HPLC (Waters Corporation, Milford, MA). The extract was injected onto a Phenomenex Luna (2) Mercury MS (20 x 2.0 mm, 5 µm) analytical column fitted with a Phenomenex C18 (4 x 2.0 mm, 5 µm) guard column (Phenomenex, Torrance, CA). A mobile phase, at a flow rate of 0.75 mL/min consisted of 10 mM aqueous ammonium acetate (A) and acetonitrile (B). Initially conditions 70 % A and 30% B were held for 0.5 min, then stepped to 2% A and 98% B and held for 1.5 minutes. Thereafter the mobile phase composition was returned to the initial conditions and held for two more minutes before the next injection. Total analysis time was 4 minutes per sample.

The liquid chromatograph was coupled to a Waters Quattro Micro mass spectrometer operated in negative electrospray ionization mode. To achieve high selectivity and sensitivity, the instrument was optimized in multiple reaction monitoring (MRM) to detect perfluorooctanoate (m/z 412.93/368.84) and internal standard (m/z 420.99/375.85). The resulting chromatograms were analyzed using MassLynx and QuanLynx software.

Calibration and quality control standards were adjusted as appropriate to cover the range required with increasing dose. The batch acceptance criteria were taken from the Guidance for Industry – Bioanalytical method validation. PFOA was reported in µM (µM = 413 ng/mL).

## **Additional Notes on Probability Analyses of Biological Indicators**

Nineteen physiological indicators were considered of interests for analyzing their probability distributions based on their PFOA level. 367 subject record entries were obtained although only 311 could be used for this analysis, as the remaining 56 did not have PFOA records. The 311 records were divided into deciles of PFOA concentrations.

The first four indicators are relevant to general category of lipid related clinical chemistries

- Low density lipoprotein LDL (Figure 6 manuscript) showed at lower PFOA concentrations, mean LDL was higher with larger variance. At higher PFOA concentrations, mean LDL was lower, with smaller variance. This difference is quite distinctive.
- Large buoyant HDL (Figure 6 manuscript) showed no strong difference between different PFOA levels.
- The total cholesterol (Figure 6 manuscript) and triglycerides (Figure S2) showed similar pattern as LDL does in Figure 6 manuscript. At lower PFOA levels, there was a higher mean and variance. At higher PFOA levels, there was a lower mean and variance.

There were three indicators relevant to renal clinical chemistries,

- For serum creatinine (Figure 11 manuscript), the only conclusion we could draw was that at higher PFOA levels, serum creatinine had a wider value range than it did at lower PFOA levels. Otherwise, differences between distributions seemed to be attributable to the intrinsic variability of creatinine.
- In most cases at lower PFOA concentrations, the means of urea (Figure S3) were also lower. At higher PFOA levels, the means of urea were also higher. There was not an observable difference between variance in urea readings across different PFOA levels.
- Serum uric acid does not vary for different levels of PFOA considering the invariance of pdfs (data not shown).

There was one indicator considered a non-specific clinical chemistry.

- The probability distributions of lactate dehydrogenase (LDH) did not show any directional trend and was characterized by strong fluctuations (data not shown).

There were five variables related to the category of liver enzymes:

- According to Figure 8 manuscript, ALT's probability density distribution was not expected to exceed 0.1 for any PFOA levels. Subjects with medium PFOA levels had the smallest variance. There was not much distinction between those with the highest and the lowest PFOA levels. Highest ALT value was 150 IU/L.
- AST (aspartate aminotransaminase) showed a slight increase for high PFOA levels (Figure S5). The underlying implication is that PFOA may not be relevant to this indicator. While comparing the minor variation between different PFOA level groups, we noticed a slight increase in mean and slight decrease in variance in the highest PFOA group, which included the subject with the highest 10% PFOA concentration.
- At any level of PFOA gamma glutamyl transaminase (GGT) (see Figure S5) did not varying much. The values of GGT spanned a wide range, up to 2000 IU/L. At

lower levels of PFOA, the range seemed to be wider than at higher levels of PFOA. At higher levels of PFOA the variance was smaller.

- Alkaline phosphatase (ALP), which corresponds to Figure S5, did not vary much across the range of PFOA levels. Similarly to GGT, the cohort variance was smaller when PFOA was high and the range was wider when PFOA was low.
- The previous 5 liver enzyme indicators presented distribution patterns similar to a Poisson distribution. For total bilirubin (BIL) (Figure S5), subjects in the medium-high PFOA range appeared to have the smallest variance.

There were three variables related to liver function (i.e., synthesis of coagulation factors).

- According to Figure S6, at higher levels of PFOA, Partial Thromboplastin Time (PTT) had a broader range, smaller mean and smaller variance. At lower levels of PFOA, the PTT had a narrower range but higher mean and variance.
- The pattern for fibrinogen (Figure S6) was also somewhat ambiguous. At higher-level PFOA levels, mean of fibrinogen was relatively lower. There was no clear distinction in variance or any other observable signatures.
- Activated Partial Thromboplastin Time (APTT) (see Figure S6) had a lower variance when PFOA levels were high.

There were two indicators under the general category of thyroid:

- TSH (thyroid stimulating hormone) (Figure 9 manuscript) demonstrated a pattern that appeared similar to a Poisson distribution. When PFOA was high, the variance in TSH was small. When PFOA was low, there was a wide range of TSH values.
- Free T4 (fT4) (Figure 9 manuscript) was one of few indicators that showed a clearer signature as PFOA concentrations varied. When PFOA was high, fT4 was higher with greater variance. When PFOA was low, fT4 was lower with smaller variance. There was a transition between the two stages.

There was no clear distinction between the lowest and highest PFOA level groups with serum amylase (data not shown). At medium levels, subjects showed smallest variance in serum amylase around the mean level of 40. Overall, variables that clearly showed more information than the others were: total cholesterol, LDL, and fT4. More questionable trends were seen for serum triglycerides, alkaline phosphatase, fibrinogen (FIB), and activated partial thromboplastin time (APTT).

## **Additional Notes on Methods**

PKPD models, like the one adopted in this manuscript, are commonly used to formally integrate available information in order to gain system-level understanding of pharmacological effects and to make informed decisions. These models are usually composed of two parts; the pharmacokinetics (PK) part representing what the body does to the drug (e.g. to understand how PFOA varies over time in the body), and the pharmacodynamics (PD) part representing what the drug does to the body (e.g. how clinical measures of exposure change over time). In this paper we used PKPD models supported by Global Sensitivity and Uncertainty Analyses (GSUA) – that is a probabilistic technique to characterize importance of model variables via propagating uncertainty in model input factors to model outputs. This provided smooth, continuous estimates of the effects of PFOA exposure beyond the discrete categories defined by the data. The information-theoretic aspect of the model lies in the idea to select the simplest form of the model and input factors to reproduce the patterns of interest. Thus, our PKPD model does not consider the whole complexity of the phenomenon (for instance the whole complexity of liver and thyroid function) – whether possible at all, because it aims to have a “macro” pattern-oriented representation of the fundamental processes to reproduce the patterns of interest simultaneously.

### **PKPD Model Calibration**

“PopED lite”, that is the computational platform used in this paper, implements standard compartmental PK models (1-, 2-, and 3-compartment models with linear and nonlinear elimination, and linear absorption), as well as commonly used PD models. For PD models, the user can alternatively input a regular mathematical expression in form of a function or an ordinary differential equation. This choice of model flexibility is chosen to cover a wide range of possible PKPD models and at the same time ensure software usability. In our study we used Eqs. 1-4 for the PKPD dynamics.

PopED lite chooses the optimization criteria from D, Ds, ED, and EDs optimal designs (Lindhardt and Gennemark, 2014) to fit the optimization need of the user. These are different optimization criterion used to estimate the probability distributions of model factors in order to calibrate the model. D-optimality seeks to maximize the determinant of the information matrix of the model design. This criterion results in maximizing the differential Shannon information content of the parameter estimates. The Fisher Information Matrix (FIM) is a way of measuring the amount of information that an observable random variable “X” carries about an unknown parameter  $\theta$  upon which the probability distribution of “X” depends. For a chosen PKPD model structure (Figure 1 manuscript), the user can specify the confidence level of the best guess of the PKPD parameters (“Step 2” in PopED lite) that in our case is suggested by the data for clinical biomarkers. If there is no uncertainty, PopED lite optimizes the experimental design using

the D optimization criterion. Otherwise, it randomly generates sets of parameters following the uniform distribution in the range specified by the user and conducts ED optimal design (by taking the expectation of the natural logarithm of the determinant of the FIM for randomly generated sets of parameters). Considering all model input factors (where model factors are both state variables and model parameters in Eqs. 1-4) along their pdfs, a Pareto frontier is determined for assessing the optimal set of values that maximize prediction accuracy with the minimum variance, or equivalently that minimize the KL divergence for all predicted patterns. The optimal model minimizes RMSE KL, and AIC for the D-optimality inferred model factors. In deterministic settings this corresponds to maximizing the concentration mean (toward observed values) and minimizing its variance. In other words the Pareto optimality criterion (Pareto, 1965) allows us to get the most accurate patterns with the least amount of information. The Pareto optimality criterion is used for the multiobjective problem to maximize prediction accuracy for multiple indicators.

A set of model input factors is on the Pareto optimal frontier if no other input set simultaneously fits all calibration patterns as well or better. The Pareto frontier approach coupled to the D optimization method eliminates the need to make input factor choices – only subject to expert knowledge – by using an intuitive and transparent notion of optimality as the basis for identifying best-fitting model input sets conditional to patterns of interest and measured information. This approach, equivalent to Maximum Entropy approaches, explores all system states by embracing the full probability space of target (or pattern) outcomes in relation to the full probability space of input factors. The identification of the Pareto set is done after assigning a probability distribution to all input factors via the D-optimization method and a full Global Sensitivity and Uncertainty Analyses (GSUA) (Ludtke et al., 2007; Saltelli et al., 2008) are performed *a posteriori* to identify variable importance and interactions for the pattern analyzed. In this paper GSUA was also used for model selection. The model input factors are calibrated for 1 week at an hour resolution and predictions are validated for the next 5 weeks of the six- week phase 1 trial.

## **Global Sensitivity and Uncertainty Analyses**

The goal of GSUA is to identify which input factors “X” in the PKPD model have the highest effect on all (and each) predicted patterns “Y” in terms of their relative importance and interdependency considering all model factor uncertainty. Because of this ability to determine model factor importance, GSUA is also used in model selection (during the calibration/validation phase) for determining the most relevant model in terms of optimal balance between model complexity, uncertainty and sensitivity that reproduces the observed PKPD patterns (concentration, cholesterol and fT4). In this paper different models correspond to different probability distribution functions assigned to the nine model

parameters to calibrate (leaving aside the state variables).  $D$ , i.e. the assigned dose, is considered as a random model factor. GSUA is applied to the discussed PKPD model introduced by Lindhardt and Gennemark (2014). With GSUA, the set of ordinary differential equations of the model can be seen as a set of stochastic differential equations in consideration of the fully probabilistic description of all input factors and their combinations according to the described dynamics. All factors are modeled as random variables distributed according to probability distributions inferred from data and expanded to consider extreme events as well as adjusted by the calibration of the PKPD model.

The initial GSUA of the PKPD model was performed by applying the Sobol method (Sobol, 1993) for a quantitative analysis of PKPD model-uncertainty propagation. The Sobol method estimates sensitivity measures which summarize the model's behavior. The most common measure of sensitivity is the first-order sensitivity index,  $S_i$ , which represents the main effect (direct) contribution of each input factor to the variance of the output. This is given by the ratio of the variance of each model factor (conditional to the predicted patterns) and the variance of the predicted patterns. The difference  $S_{ij}=1 - \sum S_i$  can be used as an indicator of the presence of interactions of model factors in the model. Thus, the total sensitivity index is defined as the sum of the relative importance and interdependency of factors.

The Sobol analysis was later improved by the information-theoretic approach of Lüdtkke et al., (2007). The first and second order sensitivity indices ( $S_i$  and  $S_{ij}$ ) are defined as the ratio of model factor entropy and mutual information (MI) with the total entropy of model outputs, respectively. MI is calculated considering factor  $X_i$  and all other in interdependent  $X_j$  conditional to "Y" (Lüdtkke et al., 2007) where "Y" is here considering the plasma concentration and effects variability (cholesterol and fT4). These indices are determined for the three predicted patterns and the average sensitivity indices are calculated considering the sensitivity values for all patterns.

These GSUA methods involve five steps: (1) the probability distribution functions (pdfs) for each input factor are selected (and later improved after the Pareto optimal calibration (Pareto, 1965)); (2) sample points are generated on the input factor distributions using the variance-based analysis (Sobol method); (3) the PKPD is executed using all sample points and a set of outputs is generated; and (4) global sensitivity analysis is performed (i.e. calculation of sensitivity indices considering variance or entropies via the Sobol and Lüdtkke approach, respectively). After step number four, other combinations or the pdfs of state variables and parameters are used and the multicriteria pattern evaluation is assessing the performance of each model. The Pareto model, after exploring all potential candidate models generates the best model and all GSUA inferred model factor importance indices.

The probabilistic PK/PD model shows that average values and other moments of pdfs capture only a subset of information about the change of biomarkers. In particular we

observe that pdfs show the non-linear change of biomarkers. Temporal trends capture only the average change of biomarkers which can lead to wrong conclusions if analyzed alone. Seemingly statistically insignificant relationships (because of the small linear regression slope or the large p-value) do not imply insignificant biological processes; these processes may be highly important considering the values of biomarkers and the change in their interdependent pdfs. Lastly, we show that by grouping observations, for meaningful toxicologically relevant categories, becomes useful in order to quantify how exposures may affect biomarkers; ensemble averages may obscure information about dose-response relationships that can be derived from the data.

## Supporting Table Captions

Table S1. Number of patients studied per cohort by the dose administered and age, height, and weight of subjects.

Table S2. Tumor site distribution and stage distribution for colorectal and pancreas.

## Supporting Figure Captions

Figure S1. Observed dynamic of total cholesterol and fT4 as a function of plasma PFOA concentration. The black and red bars in the boxes represent the median and the mean value respectively. Dots above boxes are outliers (upper dots are more than 3/2 times of upper quartile, while lower dots are less than 3/2 times of lower quartile). The extremes of the whiskers are the maximum and minimum values for each category excluding outliers. The extremes of the boxes are the third and first quartiles.

Figure S2. Pdf of serum triglycerides (TGL) for different PFOA serum concentration. TGL shows a decrease with PFOA serum concentration. The pdf of TGL became more leptokurtic from a platykurtic/bimodal pdf for higher PFOA levels; this is somewhat expected since high doses force the biology toward a more “deterministic” state where the variance of almost all biomarkers decreases slowly.

Figure S3. Pdf of urea for different PFOA serum concentrations. Urea showed an increase with PFOA serum concentration. The pdf of urea remains invariant in shape for all PFOA levels.

Figure S4. Pdf of glucose for different PFOA serum concentration. Glucose is substantially invariant across all ranges of PFOA values. A longer tail is observed for intermediate value of PFOA before PFOA starts to plateau over time.

Figure S5. Pdf of serum fibrinogen (FIB), partial thromboplastin time (PTT), and activated partial thromboplastin time (APTT) for different PFOA serum concentration. PTT showed a decrease with PFOA serum concentration. The pdf of PTT became more leptokurtic from a multimodal pdf for higher PFOA levels. FIB showed a decrease with PFOA serum concentration. The pdf of FIB became more leptokurtic from a multimodal pdf for higher PFOA levels. APTT did not show any variability with PFOA serum concentration. However, pdf of APTT became more leptokurtic and multimodal from a multimodal pdf for higher PFOA levels.

Figure S6. Pdf of alkaline phosphatase (ALP), gamma glutaminase (GGT), and total bilirubin (TBIL) for different PFOA plasma concentrations. No major difference across PFOA ranges was seen for these other clinical indicators related to liver function. In general all these indicators are higher for lower PFOA and the variance of their pdf is smaller for higher doses.

Figure S7. Pdfs of serum total cholesterol and fT4 for all patients and all patients except those using drugs for high cholesterol and hypothyroidism. No meaningful changes were observed.

Figure S8. Patterns of lipid clinical chemistries (total cholesterol, HDL and LDL) as a function of PFOA for subjects taking and not taking cholesterol lowering drugs.

Figure S9. Patterns of thyroid biomarkers (fT4 and TSH) as a function of PFOA for the cohort taking and not taking thyroxine.

Figure S10. Patterns of thyroid biomarkers (fT4 and TSH) as a function of PFOA subjects taking and not taking corticosteroids.

Figure S11. Non-linear relationship between PFOA and Dose. The observed serum concentration of PFOA increases non-linearly according to a power-law function of the dose. The inset is showing the non-linear relationships; different values of the dose correspond to different values of PFOA and the variance of this relationship is larger for larger doses.

Figure S12. Model accuracy plot. The observed and predicted serum concentrations are plotted together. The black dots are related to the average concentration of PFOA for the

multi-resolution binning that has been used (from 0 hours to 864 hours). The variability in grey is related to the Monte Carlo simulations made considering the variability of all input factors of the PKPD model.

Figure S13. Global sensitivity and uncertainty analyses of the PKPD model. GSUA is performed for the stochastic PKPD model.  $S_i$  and  $S_{ij}$  are the first and second order sensitivity indices that express the relative importance and interdependence of factors for predicting target outputs of the model (the plasma concentration of PFOA, total cholesterol and thyroid function over time). In the information theoretic GSUA equivalent relative importance (considering  $S_i$ ) between compartment effects and dose-plasma factors are found. The factor D – dose – is considered as a model factor because it enters the model as a random variable as well as other factors.  $k_a$  and  $k_e$  are power-law distributed while  $k_{12}$  and  $k_{21}$  are log-normally distributed.  $k_{10}$  is exponentially distributed.  $a$  and  $b$  are uniformly distributed.

## References

- Lindhardt, E., Gennemark, P. (2014). Automated analysis of routinely generated preclinical pharmacokinetic and pharmacodynamic data. *J. Bioinform. Comput. Biol.* **12**, 1450010.
- Lüdtke, N. S., Panzeri, S., Brown, M., Broomhead, D. S., Knowles, J., Montemurro, M. A., Kell, D. B. (2008). Information-theoretic sensitivity analysis: a general method for credit assignment in complex networks. *J. R. Soc. Interface* **5**, 223-235
- Pareto, V. (1965). *Ecrits sur la courbe de la répartition de la richesse* [Writings on the curve of the distribution of wealth] (G. Busino, Comp.). Geneva, Switzerland
- Saltelli, A., Ratto, M., Andres, T., Campolongo, F., Cariboni, J., Gatelli, D. et al. (2008). *Global Sensitivity Analysis: The Primer*. John Wiley Sons Ltd.. West Sussex, England:

Table S1.

	<i>Mean</i>	<i>Median</i>	<i>Std Dev</i>	<i>Min</i>	<i>Max</i>
<i>Age (yr)</i>	61.04	63.5	9.080052	36	76
<i>Height (m)</i>	1.6986	1.685	0.08794734	1.51	1.87
<i>Weight (kg)</i>	75.004	75.1	16.88788	46.5	123.2

Table S2.

<b>Location</b>		<b>Colorectal cancers</b>	
<i>Tumor site</i>	<i>N</i>	<i>Stage</i>	<i>N</i>
Adenocarcinoma NAS	1	Stage I	1
Breast	1	Stage II	2
Carcinoma NAS	3	Stage III	5
Cervix	1	Stage IV	4
Colorectum*	19	NA	7
Esophagus	3	Total	19
Eye	1		
Kidney	2		
Lung	2		
Neuroendocrine NAS	1		
Pancreas	7		
Pharynx	1		
Sarcoma NAS	1		
Skin	1		
Small bowel	1		
Stomach	2		
Thyroid	2		
Vulva	1		

<b>Pancreatic cancers</b>	
<i>Stage</i>	<i>N</i>
I	0
II	1
III	0
IV	3
NA	3
Total	7

\*Includes caecum

NAS: not otherwise specified

NA: not available

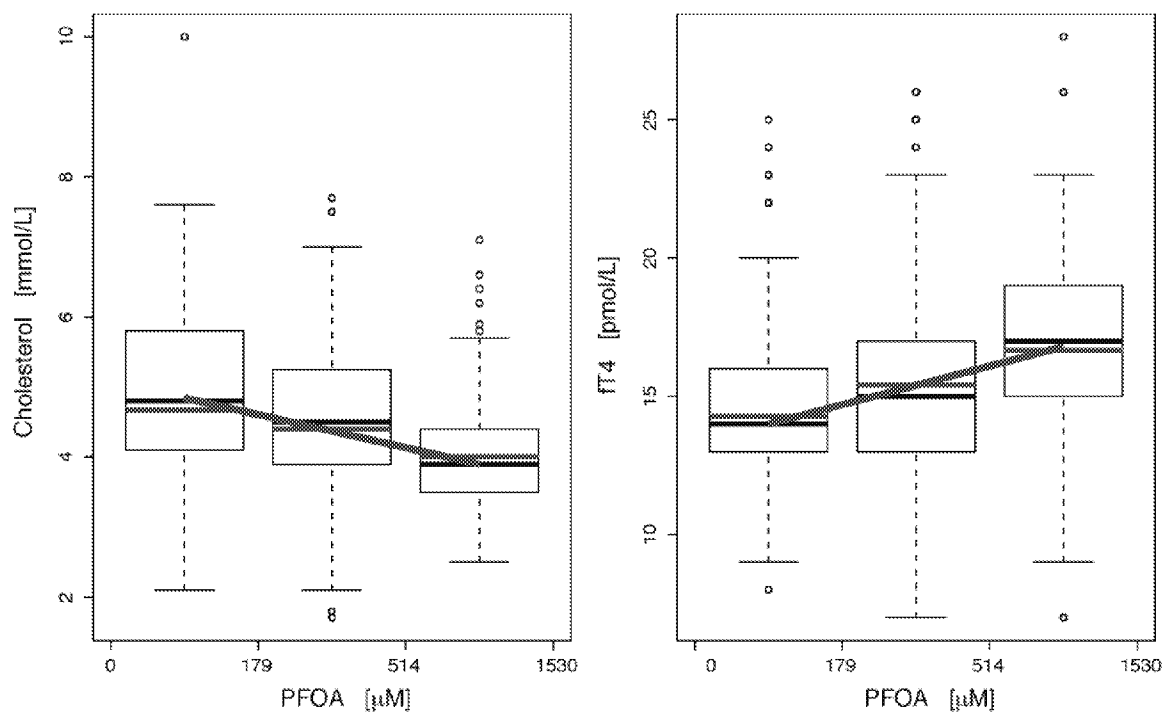


Figure S1.

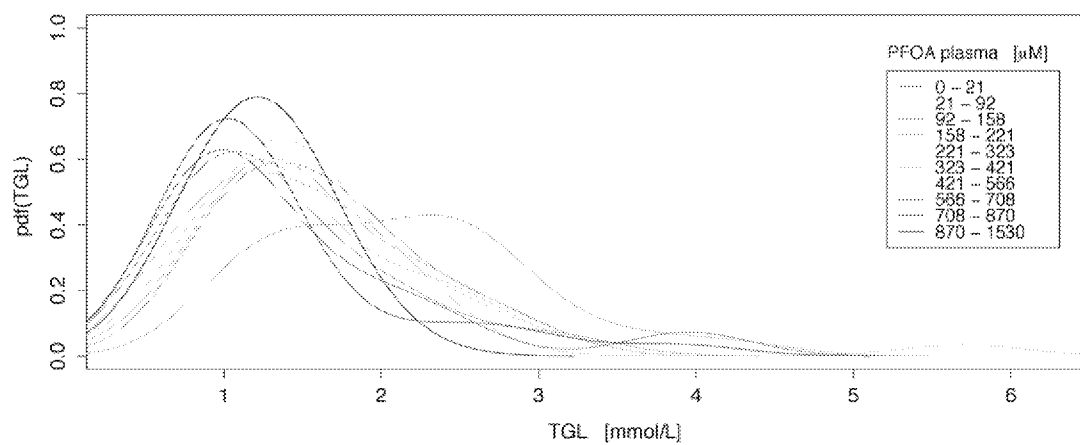


Figure S2.

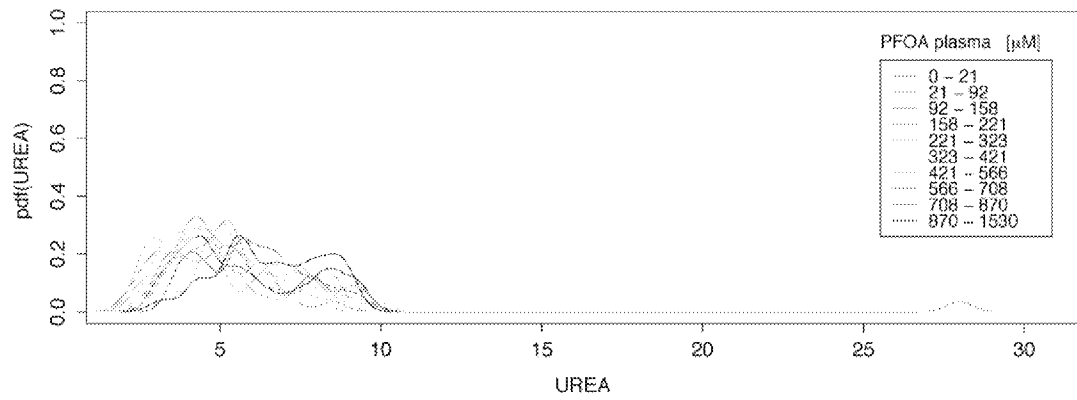


Figure S3.

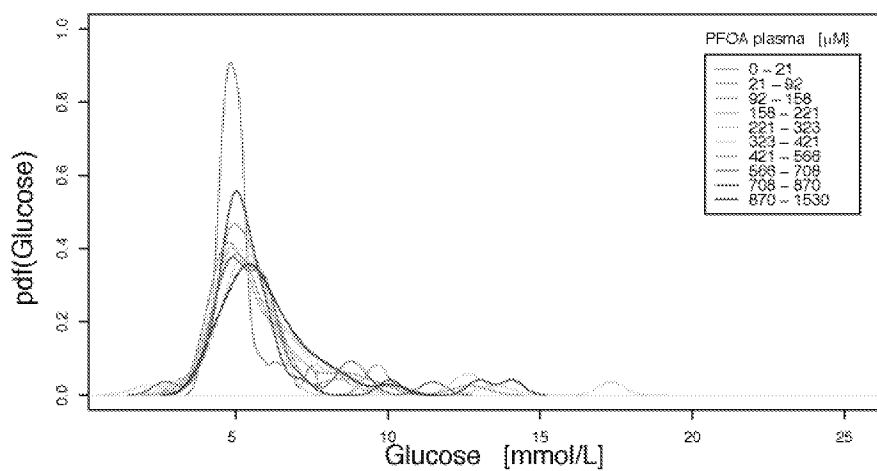


Figure S4.

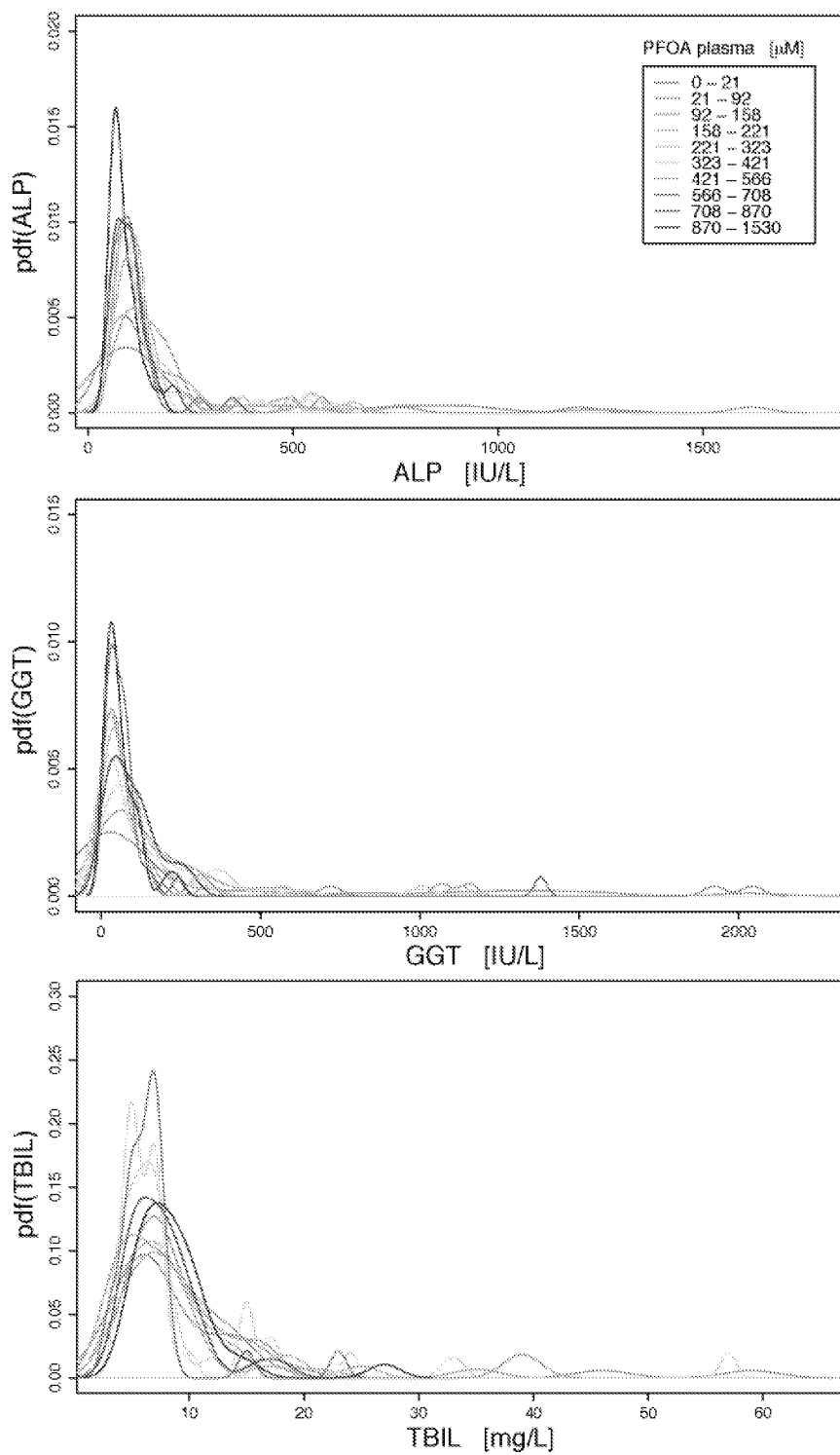


Figure S5

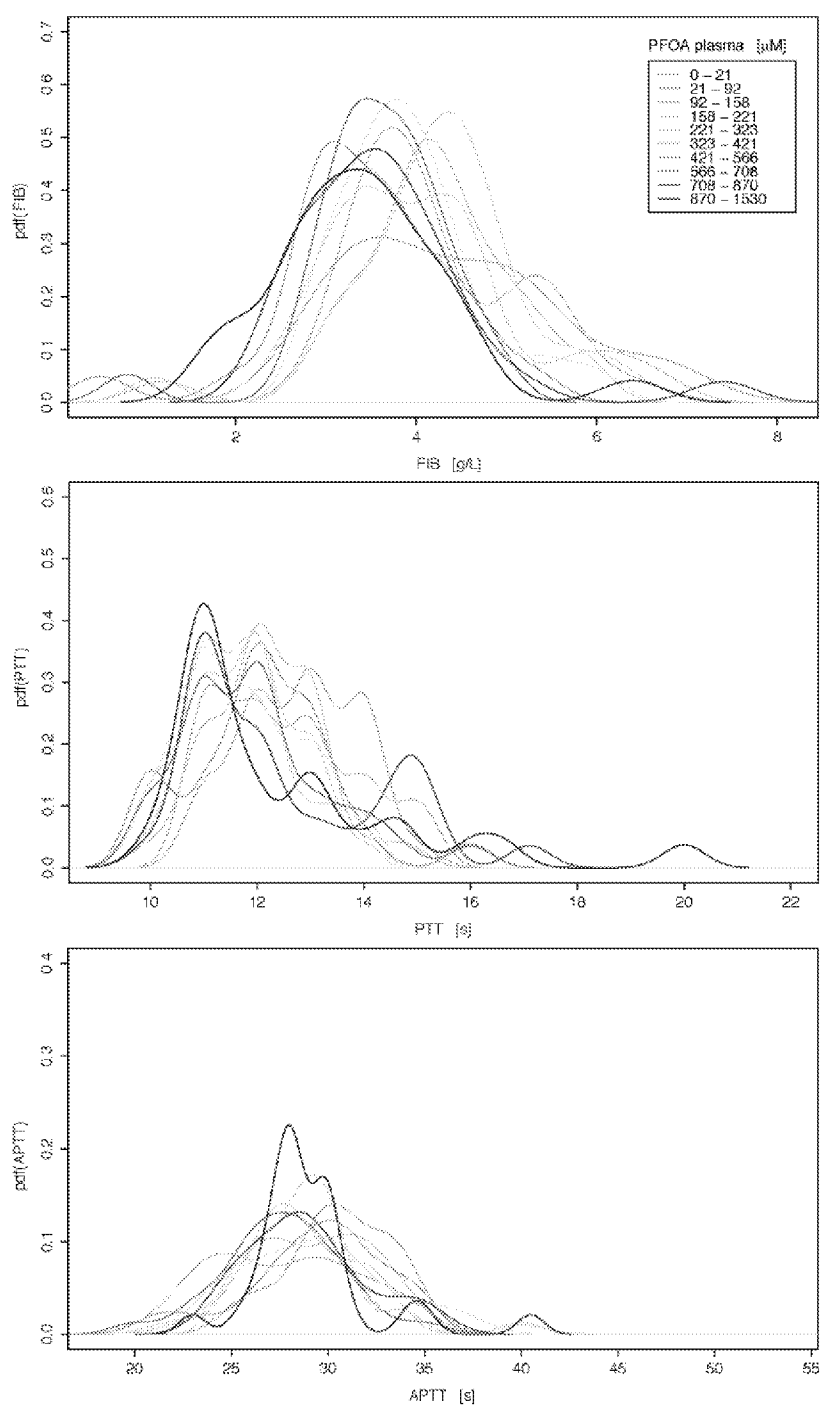


Figure S6.

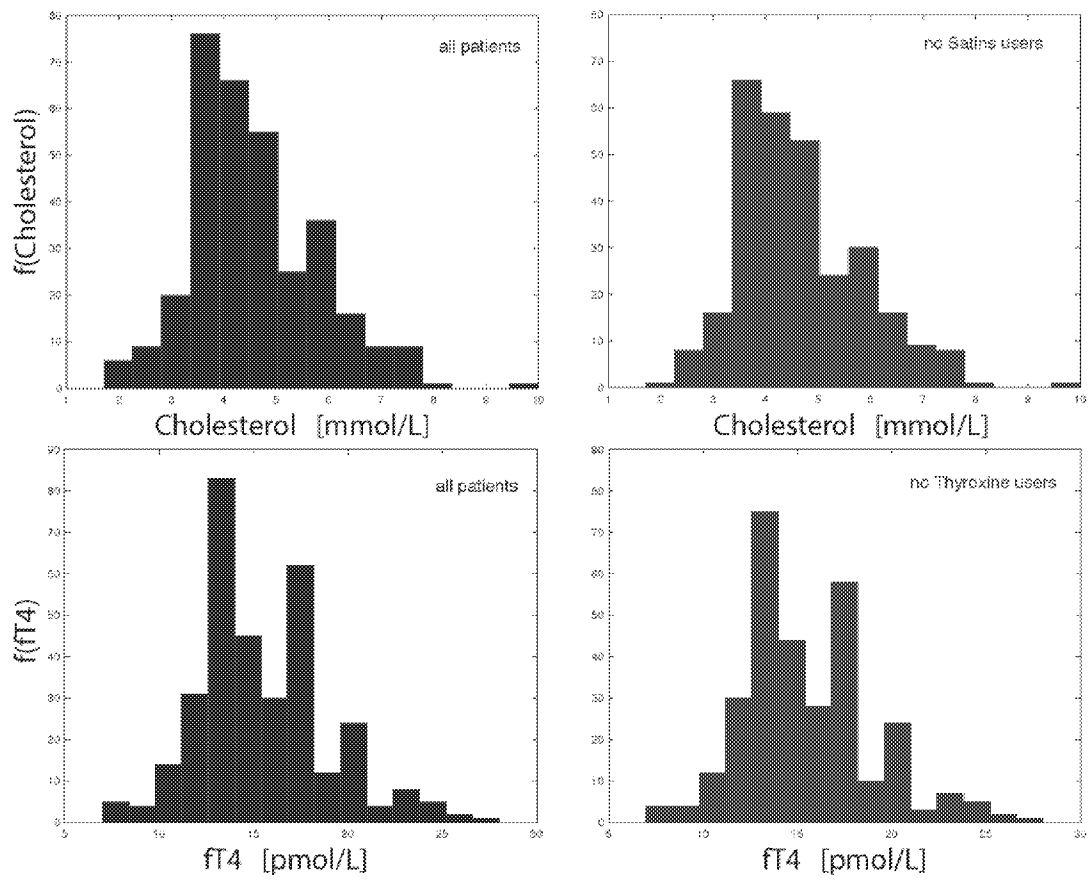


Figure S7.

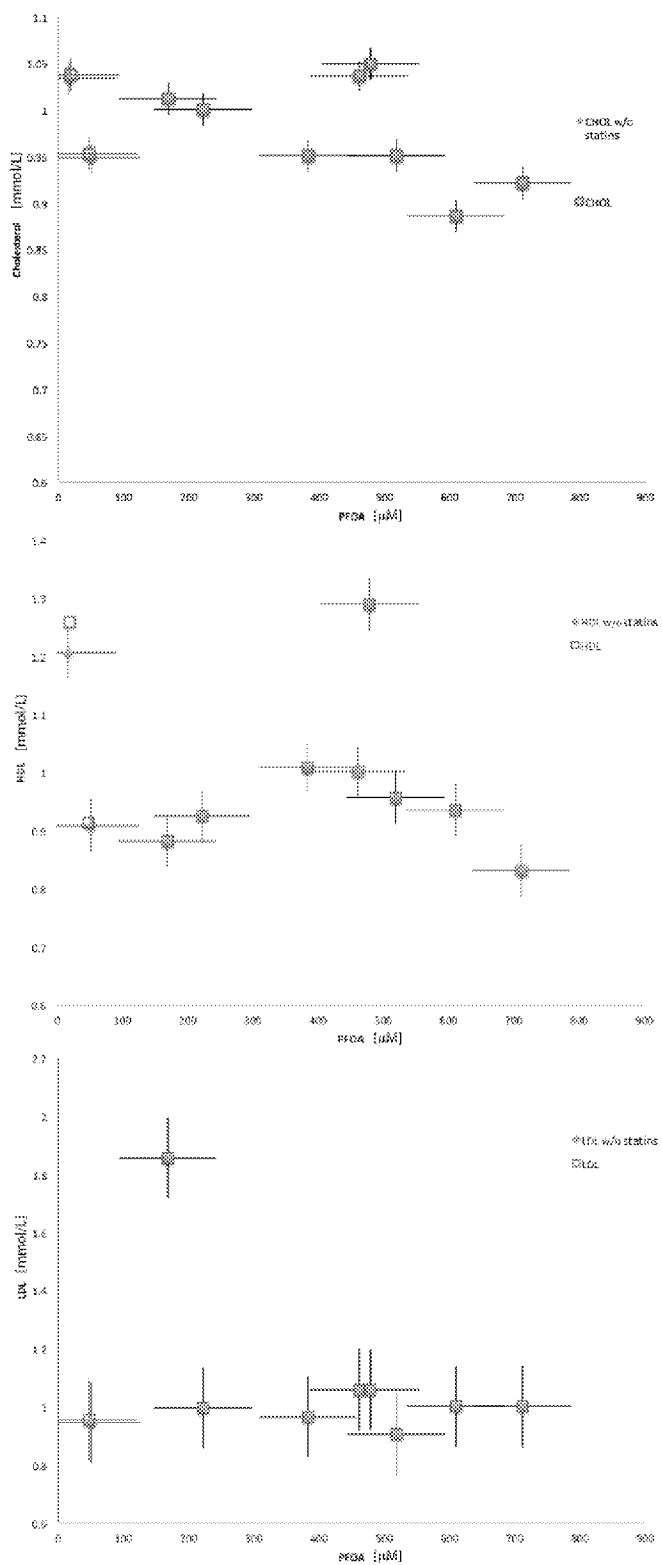


Figure S8.

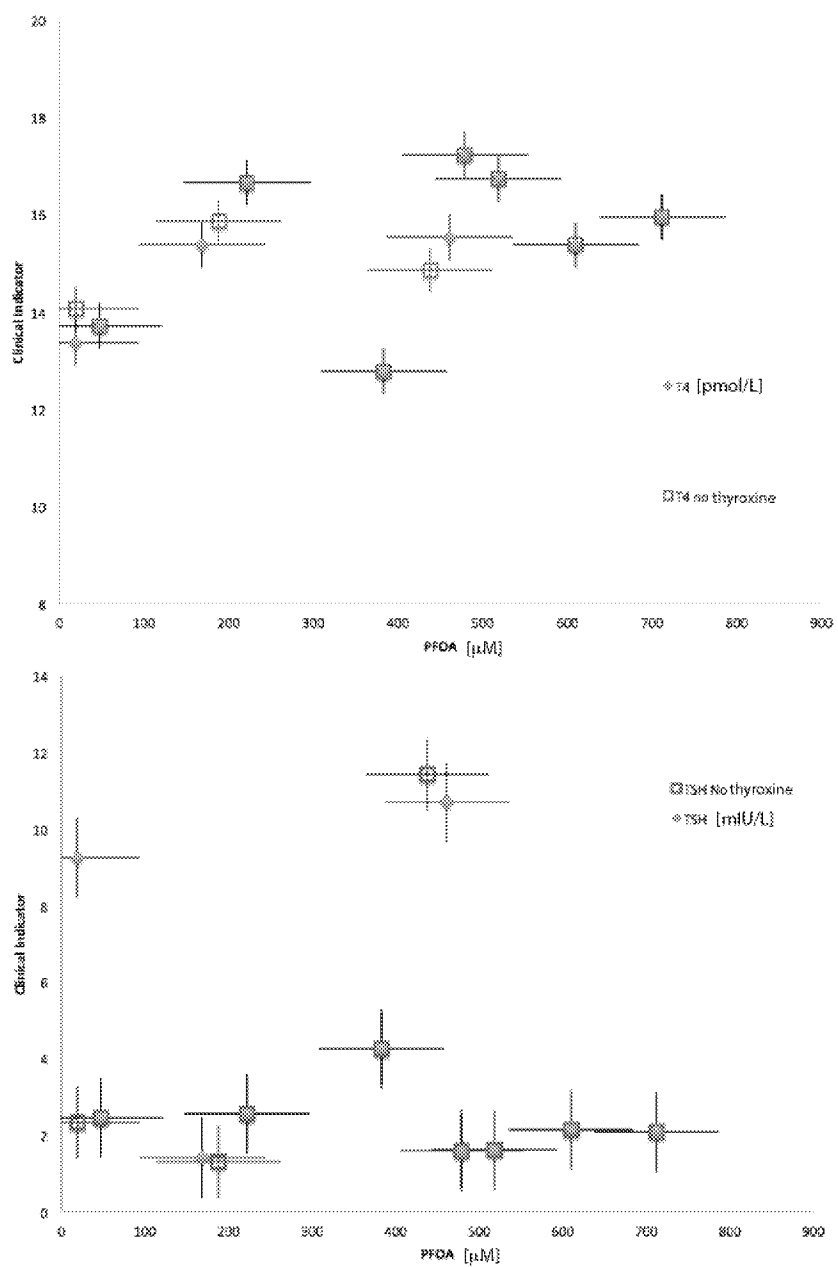


Figure S9.

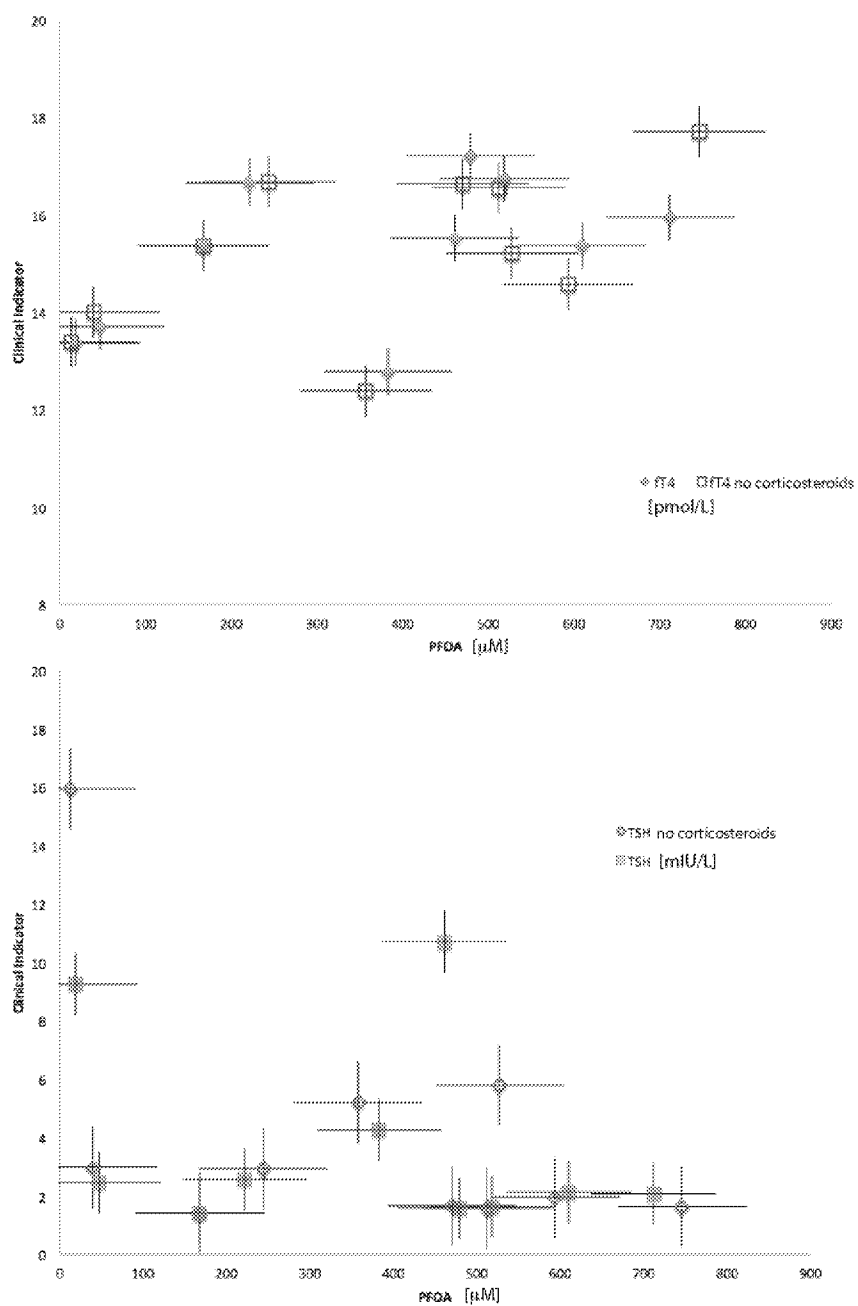


Figure S10.

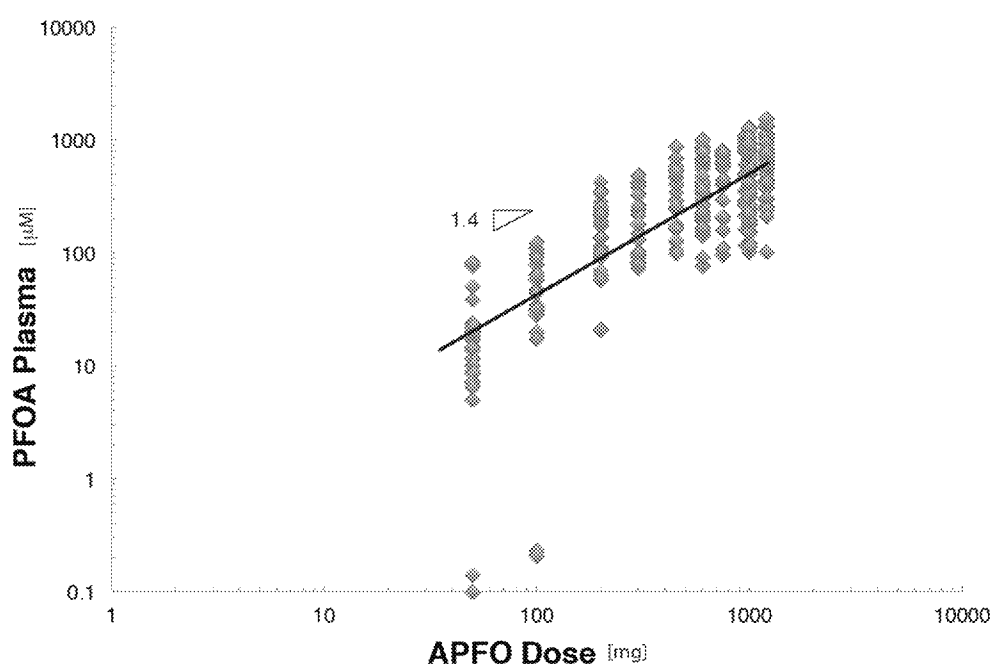


Figure S11.

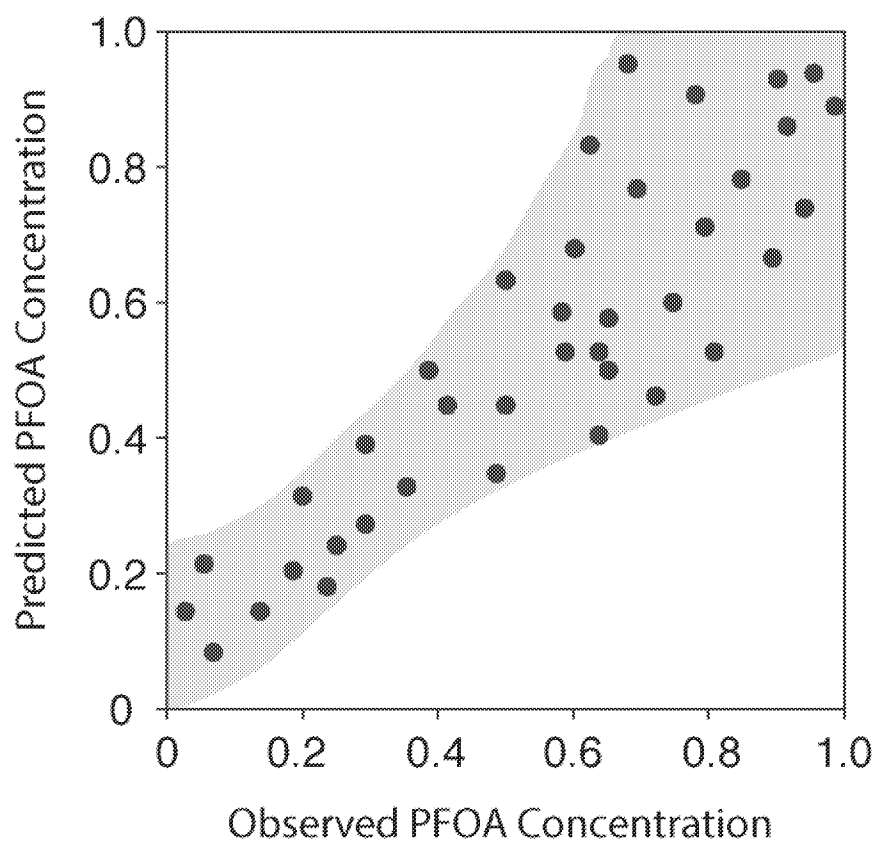


Figure S12.

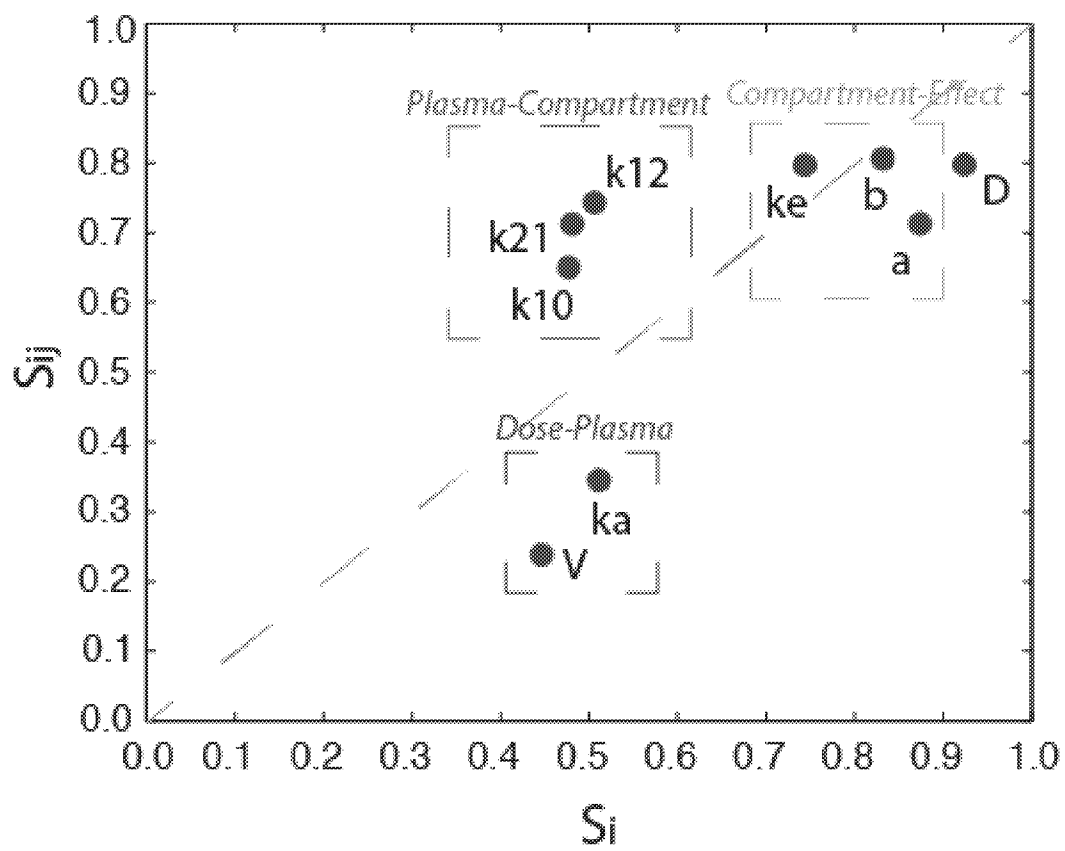


Figure S13